Cooperative Adaptive Cruise Control Safety Enhancement via Dynamic Communication Channel Selection*

Zejiang Wang, Yunhao Bai, Jingqiang Zha, Junmin Wang, Senior Member, IEEE, and Xiaorui Wang

Abstract—Adding vehicle-to-vehicle (V2V) communication into the adaptive cruise control (ACC) system produces the cooperative adaptive cruise control (CACC) with a reinforced road safety. However, current policy obliges safety-related data to be exchanged solely over the control channel (CCH) within the Dedicated Short-Range Communication (DSRC) spectrum, which may induce intolerable communication delay and higher accident risks. Standard countermeasures concentrate principally on adaptively adjusting transmission parameters. However, due to the limited network capacity of a single channel, these methods can hardly meet the real-time packet delivery requirement when vehicle density becomes high. Therefore, to ensure timely delivery of critical safety messages, this paper proposes instead a dynamic channel selection algorithm to fully exploit all the seven useable channels in the DSRC band. Experiments on a two-scaled-car platoon demonstrate the effectiveness of the method in reducing the vehicle CACC position and speed tracking errors.

I. Introduction

Combining on-board sensors, such as Lidar, radar or camera, with wireless communication devices introduces a more holistic protection for vehicle occupants. Loosely speaking, safety benefits resulting from real-time vehicle to vehicle (V2V) communication boil down to three aspects: extended information sources beyond the line of sight (LOS), anticipative warning for potential collision, and improved inter-vehicle cooperation. For instance, a pure V2V-based road intersection management system was validated in [1], where vehicle states were shared by V2V when the line of sight was obstructed. Then, the effectiveness of an electronic emergency brake light (EEBL) system, which alarms the driver to a hard brake issued from the front car in a dim environment, was demonstrated in [2]. Also, a cooperative vehicle trajectory prediction algorithm was proposed in [3], where the prediction precision was distinctly improved if neighboring vehicles' states were directly transmitted via the vehicular ad hoc network (VANET) rather than obtained from ego-car's onboard sensors. Particularly, incorporating V2V communication into adaptive cruise control (ACC) [4] leads to the cooperative adaptive cruise control (CACC) [5] with an improved safety. In contrast to ACC [6], [7], CACC can overcome the intrinsic deficiencies of embedded sensors [8], like the limited detection range and field of view, sensitivity to harsh weather and few information types. Moreover, ACC cannot guarantee the so-called *string stability* of a vehicle

*This work was supported by National Science Foundation award 1645657.

Zejiang Wang, Jingqiang Zha and Junmin Wang are with the Walker Department of Mechanical Engineering, University of Texas at Austin, Austin, TX 78712 USA (e-mail: {wangzejiang, zhajingqiang} @utexas.edu; JWang@austin.utexas.edu).

Yunhao Bai and Xiaorui Wang are with the Department of Electrical and Computer Engineering, The Ohio State University, Columbus, OH 43210 USA (e-mail: {bai.228, wang.3596}@osu.edu).

convoy due to the accumulated perception and reaction delay [9], which can amplify speed/acceleration fluctuations and consequently increase collision risks downstream the platoon. On contrary, further preview and timely perception arising out of V2V communication introduce more phase lead into the vehicle streams [10], which is able to attenuate the traffic shockwaves and maintain the string stability.

By virtue of the advantages of CACC system, extensive efforts have been made to mature this application [11], [12], [13], despite the fact that majority of literatures assumed a perfect V2V communication with neither data loss nor large communication delay. However, VANET's particular features [14], such as the harsh radio propagation condition, the fast fading channels, the hidden-terminal problem, the strong communication contention along with the highly dynamic topology, make it impractical to ignore the potential communication issues when CACC is deployed in a large scale. Actually, to alleviate the negative impact of communication delay on the performance of a CACC system, researchers from both control and communication communities have proposed various approaches. From a control viewpoint, Kalman filter was extensively utilized to estimate surrounding vehicles' states when communication networks became unreliable [15]. On the other hand, the standardized channel congestion control methods in the field of communication focused on adaptively adjusting transmission parameters [16], such as transmission power, packet sending interval, and data rate.

The current 75MHz Dedicated Short-Range Communication (DSRC) spectrum in the United States is evenly divided into seven 10MHz channels with channel 178 designated as the control channel (CCH), on which the safety-related messages are exchanged. All other six service channels (SCH), except channel 172, are retained principally for non-safety applications, such as advertisement. Instead, channel 172 will be specially reserved for future accident-avoidance applications [17], [18]. Even though the channel congestion control methods in [16] essentially mitigated packet collisions on CCH, all safety-critical information is still restricted on this single channel. When vehicle density becomes high enough and the channel contention deteriorates accordingly, the network capacity of CCH will appear insufficient due to the limited bandwidth. Reference [19] revealed that as the vehicle density increases, the average packet transmission delay on CCH augments almost exponentially. Therefore, to fundamentally reduce V2V communication delay and to further enhance the safety benefit of CACC, this paper proposes a dynamic channel selection algorithm. Instead of using one fixed channel for safety messages transmission, every vehicle in a CACC platoon independently estimates communication delays and packet delivery ratios (PDRs) of all the seven channels in the DSRC spectrum and then collaboratively selects the target

channel satisfying both the delay and PDR requirements for transmitting critical safety messages. Experiments with a platoon composed of two scaled cars were conducted to demonstrate its effectiveness.

The rest of the paper is organized as follows. The channel selection algorithm is illustrated in Section II, followed by the description of experimental scaled cars in Section III. Then, CACC experiment design and verification are shown in Section IV. Finally, Section V concludes this paper.

II. DYNAMIC COMMUNICATION CHANNEL SELECTION

The proposed dynamic channel selection algorithm makes the involved cars of a specific V2V application, e.g., CACC, under the current DSRC protocol (*IEEE 802.11p*) work collaboratively, to determine one target channel satisfying both the communication delay and PDR constraints to ensure timely transmission of crucial safety-related messages.

A. Overall Design Scheme

For simplicity, we consider a V2V use case with two involved cars. To begin with, each car locally estimates delays and PDRs of all the seven non-overlapping channels in the DSRC spectrum. Then, according to the estimated results, every involved vehicle categorizes the seven channels into three types and establishes a local channel preference list (CPL). After that, the vehicle with the greater media access control (MAC) address (acting as the sender), will send its own CPL to another car (acting as the receiver) via CCH. Subsequently, the receiver will compare sender's CPL with its own CPL to determine and switch to the optimal communication channel satisfying both the delay and PDR constraints if such a channel exists. Instead, if such a channel cannot be found due to strong channel interferences or hidden terminals, the non-safety messages transmitted by other vehicles on a suboptimal channel will be temporarily suspended to make the suboptimal channel meet the communication requirements, and this suboptimal channel will be chosen by the receiver. Thereafter, receiver's decision will be sent back to the sender in an acknowledgement (ACK) frame. Finally, based on the ACK frame from receiver, sender will also shift its channel to the target channel.

B. Delay, PDR Estimation and Channel Selection

The channel used for transmitting safety-related messages must satisfy two constraints: a packet transmitted on such a channel cannot experience a delay longer than the maximal allowable delay (MAD) and the probability of successful delivery of a single packet during the maximal allowable transfer interval (MATI) must be larger than the threshold δ . Mathematical expressions of these two constraints read:

$$\begin{cases} d \le \Delta, \\ 1 - p^{L_m} \ge \delta, \end{cases} \tag{1}$$

with d as the actual transmission delay, Δ as the maximal allowable delay, p as the probability of transmission failure of a single packet, L_m the most retransmission times within MATI. All three known parameters L_m , δ and Δ are determined by the specific V2V application such as CACC.

Based on the message collision model in [17], p of a particular channel can be computed as:

$$p = 1 - e^{-N_c \tau} e^{-N_h \tau T_v / \sigma}, \qquad (2)$$

where N_c demonstrates the number of contending nodes on the channel, N_h as the number of hidden terminals. Both N_c and N_h can be inferred from beacon messages. T_v , τ , σ , known a priori, are separately the hidden terminal vulnerable time, transmission probability in a single time slot, and the length of a time slot.

Furthermore, a transmission delay d on a specific channel consists of two parts: service delay d_s and queuing delay d_q . The queuing delay d_q can be directly obtained according to the M/G/I queue model [20]. As for the service delay d_s , by modeling the complex back-off procedure of the current DSRC protocol as a Markov process [19], d_s can be regarded as the mathematical expectation of the summation of retransmission delay, which can be calculated as:

$$d_{s} = \sum_{i=0}^{L_{u}} (1-p) p^{i} \frac{\min(2^{i} CW_{0}, CW_{\max}) E[X]}{2},$$
 (3)

with the packet error probability p indicated in (2), L_u is the default upper bound on the retransmission counts in 802.11p, CW_0 and CW_{\max} respectively are the protocol-specified initial and maximum allowable contention window, and E[X] is the mathematical expectation of time elapse until back-off counter decreased by one, which can be determined from the Markov model of DSRC's back-off procedure.

Based on (2) and (3) as well as the M/G/I queue model, the transmission delay and the packet delivery ratio on each channel can be predicted. Next, according to (1), seven channels in the DSRC band are categorized into three types, as Type1: The channel satisfies (1); Type2: The channel cannot satisfy (1) until non-safety messages transmitted by other vehicles on the channel are suspended; Type3: The channel cannot satisfy (1) even non-safety messages on the channel are suspended.

When each involved car individually categorizes the seven channels, local CPL can be constructed by assigning Type1 channels with the highest preference and Type3 channels with the lowest preference. After obtaining sender's CPL, receiver will compare it with its own CPL, and the ultimately used channel will be chosen according to the following rules: if there exist common Type1 channels for both sender and receiver, the one with the smallest N_c will be selected; else, if there exist only common Type2 channels, the one necessitating the least effort to suspend non-safety messages transmitted by other vehicles on itself will be chosen; finally, if there is neither common Type1 nor Type2 channel, the common Type3 channel suffering from the least hidden terminals will be eventually used.

Due to the space limitation, the channel selection algorithm is sketched here. Interested reader is referred to authors' previous paper [19] for a more detailed description.

III. EXPERIMENTAL HARDWARE

The channel selection algorithm in Section II was tested on a convoy with two scaled cars, exhibited in Fig. 1.

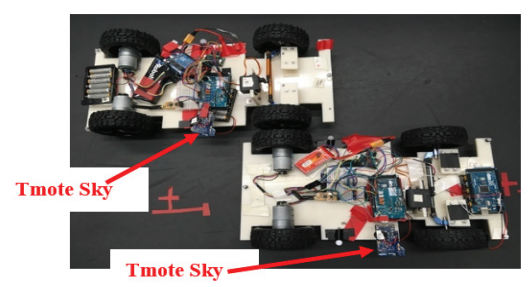


Fig. 1. Experimental scaled car.

The 1:8 scaled car was rear-wheel drive through two DC motors. Front-steering was controlled by a DC servo gear motor with accessory linkage. Arduino MEGA control board acted as the electronic control unit. To be cost-efficient, the scaled car was not equipped with any expensive sensors, such as Lidar, radar, high-precision gyroscope or accelerometer. Instead, vehicle's raw states, including longitudinal position, lateral position and yaw angle, were obtained through an image-based indoor GPS system. A radio communication (RC) module was embedded on each scaled car as a reliable GPS data receiver. Vehicle longitudinal speed and acceleration were estimated online by processing the GPS longitudinal position data via the algebraic derivative estimation technique [21], described in Section IV. In addition, as a proof of concept test bed, the V2V functionality was embodied by the off-the-shelf Tmote Sky in our laboratory instead of DSRC devices. Tmote Sky is a wireless sensor module, widely used for wireless sensor network (WSN) development. The dynamic channel selection algorithm was implemented into Tmote Sky through TinyOS operating system. As a final point, the longitudinal speed control loop of the scaled car operated within a hierarchical framework: An upper-level velocity planner calculates the desired longitudinal speed and a lower-level PID controller accomplishes the speed tracking. Estimated longitudinal speed was fed back via the RC module.

The overall longitudinal speed control architecture of the scaled car is illustrated in Fig. 2.



Fig. 2. Speed control architecture of scaled car.

IV. EXPERIMENTAL VERIFICATION

Timely delivery of information from nearby vehicles is the key to ensure that a CACC-enabled car can follow its immediate predecessor precisely and promptly [5]. A scaled-car platoon, including a leader and a follower, was used to manifest the effectiveness of the dynamic channel selection algorithm as well as the consequential control performance enhancement. Both the leading car and the following car went straight along a single lane. The leading car experienced successive acceleration and deceleration to produce speed fluctuation. The following car responded accordingly to maintain the desired distance gap. At each moment, the leading car's information was transmitted to the follower through one of the three available channels, namely CH1, CH2 and CH3, on which the quantities of contending nodes, altered by tuning the additional Tmote Sky modules around the convoy acting as interferences, were time-changing. The experiment group used the channel selection algorithm in Section II, tried to always find the optimal channel whereas the control group continued using the default CH2 (as the CCH in DSRC) to transmit information. The sending frequency was fixed as 33Hz for both cases.

A. System Modeling and Control Law Design

A vehicle platoon containing a leader and a follower (as the ego-car) is depicted in Fig. 3.

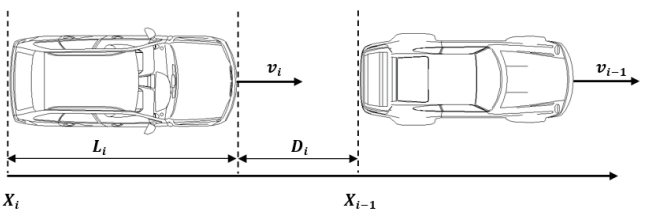


Fig. 3. CACC vehicle convoy.

The standard constant-time-headway spacing policy was used to determine the reference distance gap, as:

$$D_i = r_i + h v_i, (4)$$

with r_i as the standstill distance, h as the time headway, v_i the longitudinal velocity of ego-car. Thus, the distance tracking error reads:

$$e_i = X_{i-1} - X_i - L_i - D_i,$$
 (5)

where X_{i-1} and X_i represent rear bumper position of the preceding car and the ego-car and L_i indicates the length of the ego-car. Finally, like the case to model a full-size vehicle in [22], longitudinal dynamics of the scaled car was uniformly approximated by a first-order system as:

$$v_{i,(i-1)} + \tau_{i,(i-1)}\dot{v}_{i,(i-1)} = u_{i,(i-1)},\tag{6}$$

with $v_{i,(i-1)}$ as the actual longitudinal velocity, $u_{i,(i-1)}$ the desired longitudinal velocity, and $\tau_{i,(i-1)}$ the time constant for respectively the ego- and preceding car.

By combing (4), (5), (6), the distance error dynamics can be summarized as:

$$\begin{aligned} e_{i} &= X_{i-1} - X_{i} - L_{i} - r_{i} - hv_{i}, \\ \dot{e}_{i} &= v_{i-1} - v_{i} - h\frac{u_{i} - v_{i}}{\tau_{i}}, \\ \ddot{e}_{i} &= -\frac{\dot{e}_{i}}{\tau_{i}} - \frac{u_{i} + h\dot{u}_{i}}{\tau_{i}} + \frac{u_{i-1}}{\tau_{i-1}} - \frac{v_{i-1}}{\tau_{i-1}} + \frac{v_{i-1}}{\tau_{i}}. \end{aligned} \tag{7}$$
 Based on (7), if the desired longitudinal velocity of the

ego-car u_i satisfies:

$$u_{i} + h\dot{u}_{i} = \tau_{i} \left(\frac{u_{i-1}}{\tau_{i-1}} - \frac{v_{i-1}}{\tau_{i-1}} + \frac{v_{i-1}}{\tau_{i}} \right) + K_{d}\dot{e}_{i} + K_{p}e_{i},$$
 (8)

the error dynamics becomes:

$$\begin{bmatrix} \dot{e}_i \\ \ddot{e}_i \end{bmatrix} = \begin{bmatrix} 0 & 1 \\ -\frac{K_p}{\tau_i} & -\frac{1+K_d}{\tau_i} \end{bmatrix} \begin{bmatrix} e_i \\ \dot{e}_i \end{bmatrix}. \tag{9}$$

To make the above error matrix Hurwitz, the control gains K_p and K_d can be chosen as:

$$\begin{cases}
K_p = \xi^2 \tau_i \\
K_d = 2\xi \tau_i - 1
\end{cases}$$
(10)

with $\forall \xi > 0$. In this way, the error matrix in (9) can possess two repeated eigenvalues λ_1 , with:

$$\lambda_1 = \lambda_2 = -\xi < 0, \tag{11}$$

implying that e_i asymptotically converges to zero.

Remark: Based on (8), the ego-car only needs information from its preceding car, which matches exactly the design scheme of channel selection algorithm in Section II. Besides, since the longitudinal position and velocity of both cars are obtained from the RC module, the safety-related data transmitted via V2V merely included preceding car's desired longitudinal velocity u_{i-1} and time constant τ_{i-1} .

In addition to ensuring $\lim_{t\to\infty}e_i(t)\to 0$, a vehicle stream also obliges that the speed variation of the leading car attenuates across the vehicle string. As indicated in [23], the mathematical expression of this requirement reads:

$$\left| \frac{\tilde{X}_{i}(j\omega)}{\tilde{X}_{i-1}(j\omega)} \right| \le 1, \forall \omega, \forall i \ge 1, \tag{12}$$

where $\tilde{X}(j\omega)$ corresponds to the Laplace transform of the vehicle positions X.

Combing (4)-(9), the block diagram of the transfer function from \tilde{X}_{i-1} to \tilde{X}_i is depicted in Fig. 4, where θ represents the communication delay.

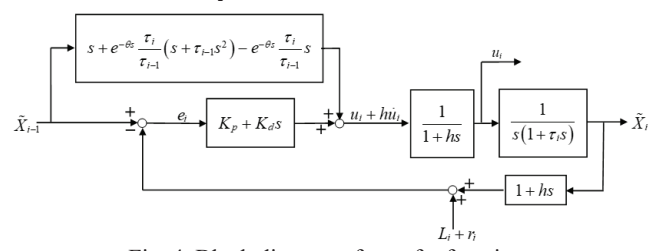


Fig. 4. Block diagram of transfer function.

Based on Fig. 4, the transfer function can be calculated as:

$$\frac{\tilde{X}_{i}}{\tilde{X}_{i-1}} = \frac{K_{p} + (K_{d} + 1)s + \tau_{i}s^{2}e^{-\theta s}}{(1 + hs)(K_{p} + (K_{d} + 1)s + \tau_{i}s^{2})}.$$
 (13)

If there does not exist any communication delay, i.e., θ =0 equation (13) is simplified as:

$$\frac{\tilde{X}_i}{\tilde{X}_{i-1}} = \frac{1}{1+hs},\tag{14}$$

implying that the string stability is intrinsically maintained. Furthermore, for a specific time headway h, there exists a maximal tolerable delay threshold θ^* , which makes (12) hold for $\forall \theta \leq \theta^*$. Fig. 5 demonstrates this $\theta^* - h$ relation with $\tau_i = 0.5$, $K_d = 0$, $K_p = 0.5$.

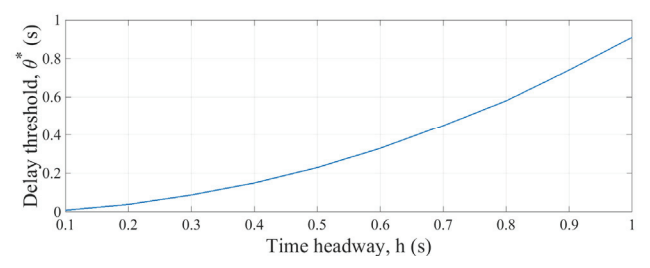


Fig. 5. Maximal tolerable delay under different headways.

B. Parameter Identification

To calculate the desired speed u_i in (8), the time constants for both ego- and preceding cars are in need. It was revealed in [13] that the time constant was virtually speed-dependent. For simplicity, only the acceleration and deceleration phases from standstill to 400 mm/s and vice versa were considered. *Matlab System Identification Toolbox* was used and an exemplary parameter identification result is demonstrated in Fig. 6.

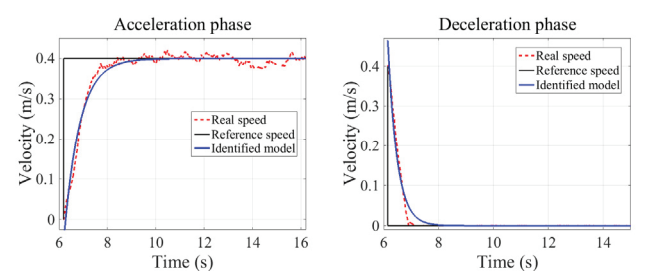


Fig. 6. Time constant identification.

The black lines in Fig. 6 indicate the step reference inputs and the red dashed lines correspond to the actual speed responses and the blue lines demonstrate the identified models. The parameter identified results are summarized in Table I.

TABLE I. TIME CONSTANT IDENTIFICATION RESULTS

	Acceleration phase Deceleration phase	
Leading car	0.65s	0.34s
Follower car	0.68s	0.30s

C. Speed and Acceleration Estimation

As indicated in Section III, raw GPS data merely contain position and yaw. However, calculating the desired longitudinal velocity u_i in (8) requires access to the actual velocity of both the ego- and the preceding cars. Commercial full-scale vehicle typically uses odometer and radar to fulfill these needs. Instead, for the scaled cars, v_i and v_{i-1} were obtained by analyzing raw GPS position data. Pure differentiator cannot be used straightforwardly because of signal noise. Rather, the algebraic differentiation estimator (ADE) in [21] was utilized to determine velocities in real time.

ADE is a robust, model-independent, and purely algebraic signal differentiator. It uses weighted *integrations* of original signal to calculate its arbitrary-order *derivatives*. The expressions of the zero-, first- and second-order estimated derivatives of a noisy signal v(t) are:

$$\begin{cases} \hat{y}(t) = \frac{2}{T^2} \int_0^T (2T - 3\tau) y(t - \tau) d\tau \\ \hat{y}(t) = \frac{6}{T^3} \int_0^T (T - 2\tau) y(t - \tau) d\tau \end{cases}, \quad (15)$$

$$\hat{y}(t) = \frac{60}{T^5} \int_0^T (T^2 - 6T\tau + 6\tau^2) y(t - \tau) d\tau$$

where T corresponds to the estimation window length. When (15) is digitally implemented, higher-order derivative estimation requires a relatively larger T to better annihilate high-frequency noise and to further mitigate the intrinsic numerical integration error. Exemplary signal filtering and derivative estimation results are demonstrated in Fig. 7, with

T fixed as 0.1 second for zero- and first-order estimations and 0.3 second for second-order derivative estimation.

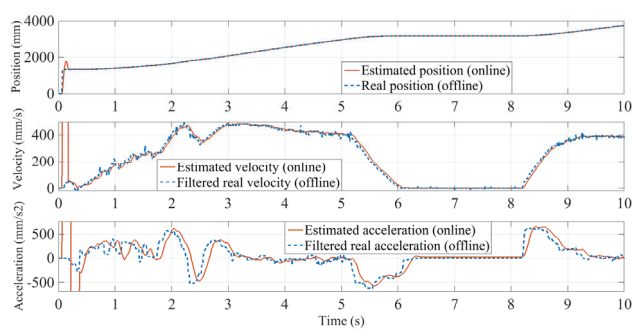


Fig. 7. Algebraic estimation result.

In Fig. 7, the red solid lines correspond to the online filtered/estimated variables and the dashed blue lines represent the real variables which were either directly measured or post-processed offline. Clearly, both the filtered position and the estimated velocity fitted well with the real data. Per contra, there existed a distinct phase lag in the estimated acceleration, owing to its relatively large estimation window. However, estimated acceleration was not involved in calculating the desired speed. Instead, it was solely used for experiment demonstration purpose in the next subsection.

D. Experiment Results

The time-changing numbers of interferences on the three available channels CH1, CH2 and CH3 were listed in Table II.

TABLE II. NUMBERS OF INTERFERENCES ON AVAILABLE CHANNELS.

	t < 6.5	$6.5 \le t < 10$	$10 \le t < 13.5$	<i>t</i> ≥13.5
CH1	5	10	1	3
CH2	9	5	8	2
СН3	1	0	6	10

At each instant, there were in total 15 interfering nodes distributed unevenly on the three channels. The shaded block in each column of Table II indicates the least number of interferences on all the three useable channels, and the channel selection result is demonstrated in Fig. 8.

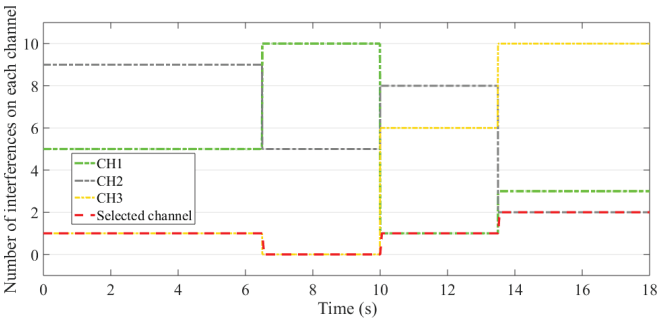


Fig. 8. Channel selection result.

Certainly, the selected channel (red dashed line) always corresponded to the optimal one with the least interferences, proving the efficiency of the channel selection algorithm.

Then, the distance tracking errors (5) when either the selected channel or the default CH2 was utilized are demonstrated in Fig. 9. In Fig. 9, the red dashed line shows the distance tracking error when the default crowded CH2 was used whereas the blue solid line corresponds to the result with

the dynamically selected channel. Evidently, V2V communication via the default CH2 entailed a more drastic and mutable distance tracking error, giving rise to a higher collision risk. On the contrary, using dynamically selected channel limited the range of distance tracking error within ± 150 mm.

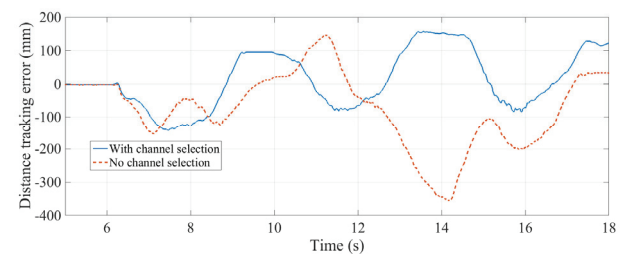


Fig. 9. Distance tracking error.

Further, the preferred disturbance attenuation character of a platoon can be verified by comparing the longitudinal velocity and acceleration of each car. Fig. 10 shows the longitudinal velocities of both the leading and the follower car with either the selected channel or the default CH2 applied.

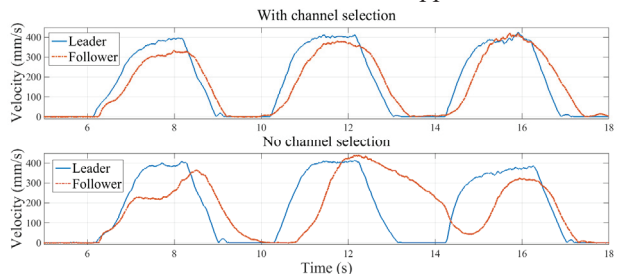


Fig. 10. Vehicle longitudinal velocities.

The upper/lower plot in Fig. 10 represents separately the velocities with the dynamically selected channel/the default CH2 used for V2V communication. Hence, applying the selected channel ensured that the velocity tracking error of the leading car was not amplified. On the contrary, a huge delay issued from the contention-extensive CH2 generated a sluggish and amplified velocity response of the follower car.

Further, the absolute relative speed $|v_{leader} - v_{follower}|$ is presented in Fig. 11.

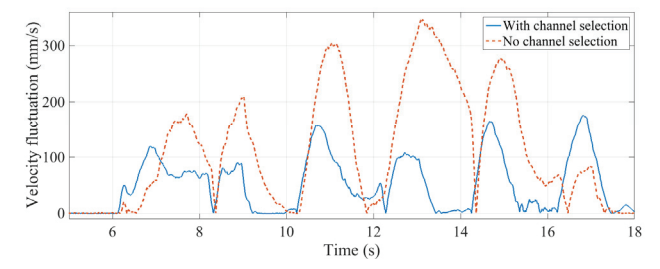


Fig. 11. Relative speed.

The red dashed/blue solid line individually features the result when the default CH2/dynamically selected channel was used. Hence, conspicuous velocity fluctuation can be witnessed when CH2 was employed. In contrast, using the selected channel made the following car response swiftly, leading to a mild speed fluctuation.

At last, the longitudinal accelerations of both cars are exhibited in Fig. 12.

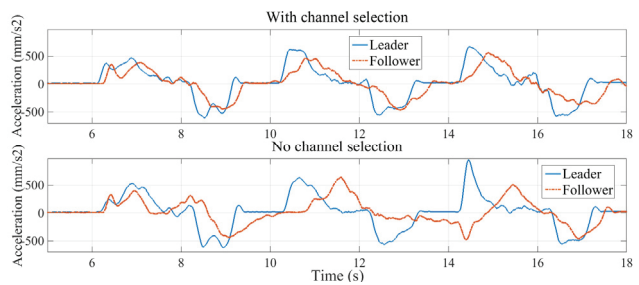


Fig. 12. Vehicle longitudinal acceleration.

The results with/without channel selection are depicted separately in the upper- and lower-plot of Fig. 12. Thus, the acceleration of the leading car was not amplified during all the three accelerating phases by use of the selected channel. Instead, with the fixed CH2, the maximal acceleration of the follower $(0.640\,m/\,s^2)$ at 11.5s was greater than the maximal acceleration of the leader $(0.628\,m/\,s^2)$ at 10.6s during the second accelerating phase.

Remark: Two scaled cars were involved in the experiments. Simulation results in terms of communication delay and PDR with multiple-car scenarios can be found in [19].

V. CONCLUSIONS

Current DSRC protocol restricts exchange of safety-related messages through only one channel, which can induce huge transmission delay and safety risk when V2V deploys in a large scale. Therefore, a dynamic channel selection algorithm is proposed in this paper to exploit all the seven channels in the DSRC spectrum for in time safety data transmission. Experiments under a CACC scenario with two scaled cars demonstrated its effectiveness. Scenarios with more involved cars will be tested in the next step.

REFERENCES

- [1] J. Ibanez-Guzman, S. Lefevre, A. Mokkadem, and S. Rodhaim, "Vehicle to vehicle communications applied to road intersection safety, field results," in *IEEE Conference on Intelligent Transportation Systems (ITSC)*, Madeira Island, Portugal, 2010, pp. 192–197.
- [2] M. Shulman and R. Deering, "Vehicle safety communications in the United States," in *Conference on Experimental Safety Vehicles*, 2007.
- [3] P. Lytrivis, G. Thomaidis, M. Tsogas, and A. Amditis, "An advanced cooperative path prediction algorithm for safety applications in vehicular networks," *IEEE Transaction on Intelligent Transportation System*, vol. 12, no. 3, 2011, pp. 669–679.
- [4] L. Xiao and F. Gao, "A comprehensive review of the development of adaptive cruise control systems," *Vehicle System Dynamics*, vol. 48, no. 10, 2010, pp. 1167–1192.
- [5] S.E. Shladover, C. Nowakowski, X.Y. Lu and R. Ferlis, "Cooperative adaptive cruise control: Definitions and operating concepts," *Transportation Research Record: Journal of the Transportation Research Board*, (2489), 2015, pp. 145–152.
- [6] J. Wang and R. Rajamani, "Should Adaptive Cruise Control Systems Be Designed to Maintain a Constant Time-Gap between Vehicles?" IEEE Transactions on Vehicular Technology, Vol. 53, Issue 5, pp. 1480 – 1490, September 2004.
- [7] J. Wang and R. Rajamani, "The Impact of Adaptive Cruise Control Systems on Highway Safety and Traffic Flow," Journal of Automobile Engineering, Proceedings of the Institution of

- Mechanical Engineers, Part D, Vol. 218, Issue 2, pp. 111 130, 2004.
- [8] G. Xiong, H. Li, Y. Jin, J. Gong and H. Chen, "Collision avoidance system with cooperative adaptive cruise control in highway entrance ramp environment," in 2017 18th International Conference on Advanced Robotics (ICAR), Hong Kong, China, 2017, pp. 549–553.
- [9] S.E. Shladover and V. Milanés, "Modeling cooperative and autonomous adaptive cruise control dynamic responses using experimental data," Transportation Research Part C: Emerging Technologies, (48), 2014, pp. 285–300.
- [10] P. A. Cook, "Stable control of vehicle convoys for safety and comfort," IEEE Transaction on Automatic Control, vol. 52, no. 3, 2007, pp. 526–531.
- [11] V. Milanés, S.E. Shladover, J. Spring, C. Nowakowski, H. Kawazoe, and M. Nakamura, "Cooperative Adaptive Cruise Control in Real Traffic Situations," IEEE Transaction on Intelligent Transportation System, vol. 15, no. 1, 2014, pp. 296–305.
- [12] S. Kato, S. Tsugawa, K. Tokuda, T. Matsui and H. Fujii, "Vehicle control algorithms for cooperative driving with automated vehicles and intervehicle communications," IEEE Transaction on Intelligent Transportation System, vol. 3, no. 3, 2002, pp. 155–161.
- [13] K. Lidström et al., "A modular CACC system integration and design," IEEE Transaction on Intelligent Transportation System, vol. 13, no. 3, 2012, pp. 1050–1061.
- [14] F. Cunha et al., "Data communication in VANETs: Protocols, applications and challenges," Ad Hoc Networks, vol. 44, 2016, pp. 90–103.
- [15] Z.A. Biron, S. Dey and P. Pisu, "Sensor fault diagnosis of connected vehicles under imperfect communication network," in ASME 2016 Dynamic Systems and Control Conference (DSCC), Minneapolis, Minnesota, 2016, pp. V001T16A003-V001T16A003.
- [16] M. Sepulcre, J. Mittag, P. Santi, H. Hartenstein and J. Gozalvez, "Congestion and awareness control in cooperative vehicular systems," Proceedings of the IEEE, vol. 99, no. 7, 2011, pp. 1260–1279.
- [17] D. Jiang, V. Taliwal, A. Meier, W. Holfelder and R. Herrtwich, "Design of 5.9 GHz DSRC-based vehicular safety communication," IEEE Wireless Communications, vol. 13, no. 5, 2006, pp. 36–43.
- [18] J.B. Kenney, "Dedicated short-range communications (DSRC) standards in the United States," Proceedings of the IEEE, vol. 99, no. 7, 2011, pp. 1162–1182.
- [19] Y. Bai, K. Zheng, Z. Wang, X. Wang and J. Wang, "Dynamic channel selection for real-time safety message communication in vehicular network," in IEEE Real-Time Systems Symposium (RTSS), TN, USA, 2018, pp. 56-66.
- [20] Y. Yao, L. Rao and X. Liu, "Performance and reliability analysis of IEEE 802.11 p safety communication in a highway environment," IEEE Transaction on Vehicular Technology, vol. 62, no. 9, 2013, pp. 4198–4212.
- [21] M. Fliess, C. Join and H. Sira-Ramirez, "Non-linear estimation is easy," International Journal of Modelling, Identification and Control, vol. 4, no. 1, 2008, pp. 12–27.
- [22] J. Ploeg, B.T. Scheepers, E. Van Nunen, N. Van de Wouw and H. Nijmeijer, "Design and experimental evaluation of cooperative adaptive cruise control," in *IEEE Conference on Intelligent Transportation Systems (ITSC)*, Washington DC, USA, 2011, pp. 260–265.
- [23] G. Naus, R. Vugts, J. Ploeg, M. Van de Molengraft and M. Steinbuch, "Towards on-the-road implementation of cooperative adaptive cruise control," in *Proc. 16th World Congr. Exhib. Intell. Transp. Syst. Serv*, 2009.